Bulgarian Chemical Communications, Volume 40, Number 3 (pp. 267–276) 2008

Conduction mechanism of anodic oxide films on tungsten – effect of the electrolyte pH

V. I. Karastoyanov, M. S. Bojinov*

Department of Physical Chemistry, University of Chemical Technology and Metallurgy, 8 Kliment Ohridski Blv., 1756 Sofia, Bulgaria

Received October 25, 2007; Revised February 9, 2008

The anodic oxidation of tungsten has been studied in 1M sulphate solutions with pH ranging from 0 to 5 containing 0.1 M of fluoride as HF or NaF. Steady-state currents measured in the potential range 0.1 to 4 V vs. SCE increase with pH, indicating enhanced dissolution of the film, which is a necessary precursor reaction for the formation of a nanoporous oxide structure. Thus, the effect of fluoride on the steady-state current density is more pronounced in weakly acidic solutions, indicating that such electrolytes are probably more promising for the fabrication of nanotube arrays of WO_3. The electrochemical impedance response in the passivation and passivity ranges is dominated by the processes in the barrier layer and at its interface with the electrolyte. The presence of a pseudo-inductive loop in the impedance spectra at intermediate frequencies indicates point defect interaction during film growth and dissolution processes. Further, a low frequency time constant can be related to the passivation process itself. A kinetic model including a recombination reaction between positively and negatively charged point defects at the film/solution interface and a kinetic scheme for tungsten oxidation/dissolution at the same interface is found to reproduce satisfactorily the steady-state currents and the impedance spectra depending on the potential. Such a model for the conduction mechanism in the barrier layer is believed to be an essential part of a modelling approach to the formation of the nanoporous overlayer.

Key words: Tungsten; Sulphate-Flioride Electrolyte; Anodic films; Oxides; Point defects; Impedance spectroscopy.

INTRODUCTION

There have been numerous attempts to improve further the performance of Pt–type electrocatalysts for methanol oxidation using a wide variety of two- and multicomponent systems. A promising method for enhancing oxidative reactivity is a combination of Pt-based systems with large-surface-area nanocrystalline inorganic oxide matrices that would ensure the metal-support interactions, a homogeneous distribution of catalytic sites, facilitated charge distribution and overall stability [1, 2]. Among applicable inorganic compounds, tungsten oxide seems to promote electrocatalytic oxidation of methanol by interacting with Pt via hydrogen spillover or through the formation of highly conductive tungsten bronzes [3–9]. In addition, tungsten oxide has been receiving considerable attention in recent years because of its NO_x, CO, and H_2S gas sensing properties [10, 11] as well as for its use in electrochromic [12–19], photochromic [20, 21] and transparent conducting electrode applications [22, 23]. Therefore, our interest is in developing a relatively simple route of producing ordered nanoporous tungsten oxide structures based on anodization. Anodization of W to produce compact barrier-type oxides has been reported by numerous authors during the last 30 years [24–55]. It has been found out that the film composition is very close or practically identical with WO_3. The anodic film is a wide band-gap amorphous semiconductor (mobility gap, 2.8–3.1 eV), and the donor concentration as estimated based on Mott-Schottky analysis has been found to depend on the film thickness. Photoelectrochemical impedance and transient measurements point to a major role of the first layer near the film/electrolyte interface in the kinetics of electron-hole recombination via surface states [40, 41]. In-situ thickness versus time measurements have indicated that dissolution of the oxide plays an important role during film growth and that the process of thickness increase is controlled by interfacial processes rather than conduction in the bulk oxide [54]. The formation of ordered nanoporous anodic oxides on W has been reported recently during oxidation in oxalic acid [56] and in sulphate-fluoride electrolytes [57] at comparatively low voltages, whereas a possibility of fast growth of oxide nanotubes promoted by oxide breakdown in chloride or perchlorate electrolytes at higher voltages has also been demonstrated [58]. In the

* To whom all correspondence should be sent:
E-mail: martin@uctm.edu

present paper, we report electrochemical measurements of the formation and properties of the anodic oxide on W in sulphate-fluoride solutions with pH 0–5. Steady-state current versus potential curves and electrochemical impedance spectroscopic measurements have been employed to characterize the individual steps of the overall oxidation reaction that are detectable by electrochemical means. The impedance spectra as depending on the potential and fluoride concentration have been quantitatively interpreted by a kinetic model featuring ionic defect recombination and an elaborated scheme for the oxidative dissolution of tungsten at the film/electrolyte interface [45, 46]. The main kinetic, transport and structural parameters characterizing the conduction mechanism in the oxide have been estimated as depending on electrolyte pH.

EXPERIMENTAL

The working electrode material was pure W (99.9%, Goodfellow). Disc shaped cuts of that material were insulated with epoxy resin and inserted in PTFE holders in order to expose an area of 0.00785 cm^2 to the electrolyte. The working electrodes were mechanically abraded with emery paper up to grade 2400, rinsed with bidistilled water and dried by hot compressed air. The electrolytes (1 M SO_4^{2-} + 0.1 M F^-) were prepared from reagent purity grade H_2SO_4, Na_2SO_4 and NaF with pH from 0 to 5. A conventional electrolytic cell was employed featuring a large area Pt mesh counter electrode and a saturated calomel reference electrode. All the potentials in the present paper are given *versus* this electrode. Measurements were performed at room temperature (20 ± 1ºC) in naturally aerated solutions. The current *versus* potential curves and impedance spectra in the range 0.1–4.0 V vs. SCE have been measured using an Autolab PGSTAT30/FRA potentiostat driven by GPES and FRA2 software (EcoChemie). After a steady-state current was reached, impedance spectra have been registered in the frequency range 20 mHz to 50 kHz at an a.c. amplitude of 15 mV. The linearity of the impedance spectra was checked by measuring spectra at a.c. amplitudes ranging from 5 to 20 mV. The causality of the spectra was verified by a Kramers-Kronig compatibility test, embedded in the measurement software. For the fitting and simulation of impedance spectra, Origin 7.5 based routines were employed.

RESULTS

Current vs. potential curves

The current versus potential curves were measured in the potential range from 0.1 to 4 V in order to characterize the active-to-passive transition and the passive range of W. Figure 1 shows current versus potential curves of W measured in 1M SO_4^{2-} + 0.1 M F^- solutions with pH from 0 to 5.

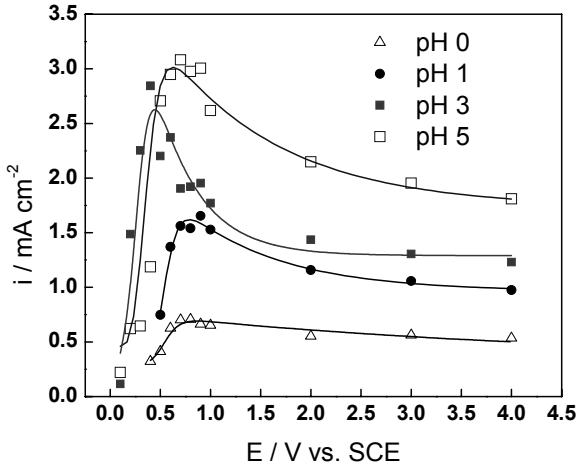

Fig. 1. Steady state current density versus potential of W in 1 M SO_4^{2-} + 0.1 M F^-, pH 0 to 5. Points – experimental data, solid lines – best-fit calculation according to the proposed model.

The active-to-passive transition is observed in the potential range 0.4–1.0 V and it is the more pronounced, the higher the pH of the solution is. In other words, the passivation current density is larger at higher pH and the difference in magnitude between the passivation current density and the current density in the passive state is also larger. This fact indicates that the dissolution of W through the oxide is favoured by pH increase. On the other hand, there is no systematic dependence of the passivation potential on pH, which probably means that the nature of the rate-limiting steps of the overall reaction is not altered by the decrease of the acidity of the solution. In the passive range (above 1 V), the current density slightly decreases with increasing potential and reaches constant values. On the overall, in this region the current density is only slightly dependent on the potential, indicating that the chemical dissolution of the oxide is probably the rate-controlling step of the overall oxidation process. The steady-state current in the passive state increases with pH indicating an apparent reaction order of the chemical dissolution reaction close to 0.5.

Impedance spectra

The impedance spectra for the W/WO_3/1M SO_4^{2-} + 0.1 M F^- system at two different pH in the passivetion region (0.4–1.0 V) are presented in Figs. 2–3.

The impedance magnitude at low frequencies $Z_{f\to 0}$ decreases significantly with increasing pH, in line with the increase in the current density (Fig. 1).

On the other hand, at potentials above the active-to-passive transition $Z_{f\to 0}$ increases with increasing potential, as it is observed also by other authors in a range of solutions [44, 45, 52]. This trend most probably reflects the influence of the film thickness (which increases linearly with potential, as it is well known for oxide growth on valve metals) on the impedance magnitude [44, 45, 52].

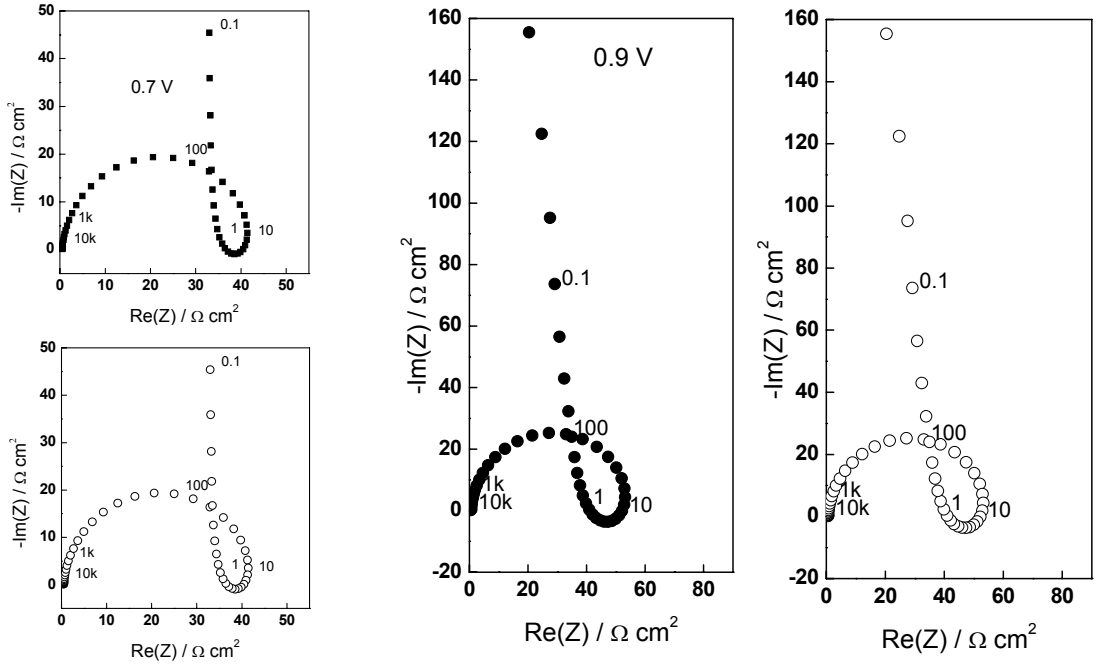

Fig. 2**.** Impedance spectra of W in 1 M SO_4^{2-} + 0.1 M F^-, pH 1 solution at 0.7 and 0.9 V. Closed symbols – experimental data, open symbols – best-fit calculation according to the proposed model. Parameter is frequency in Hz.

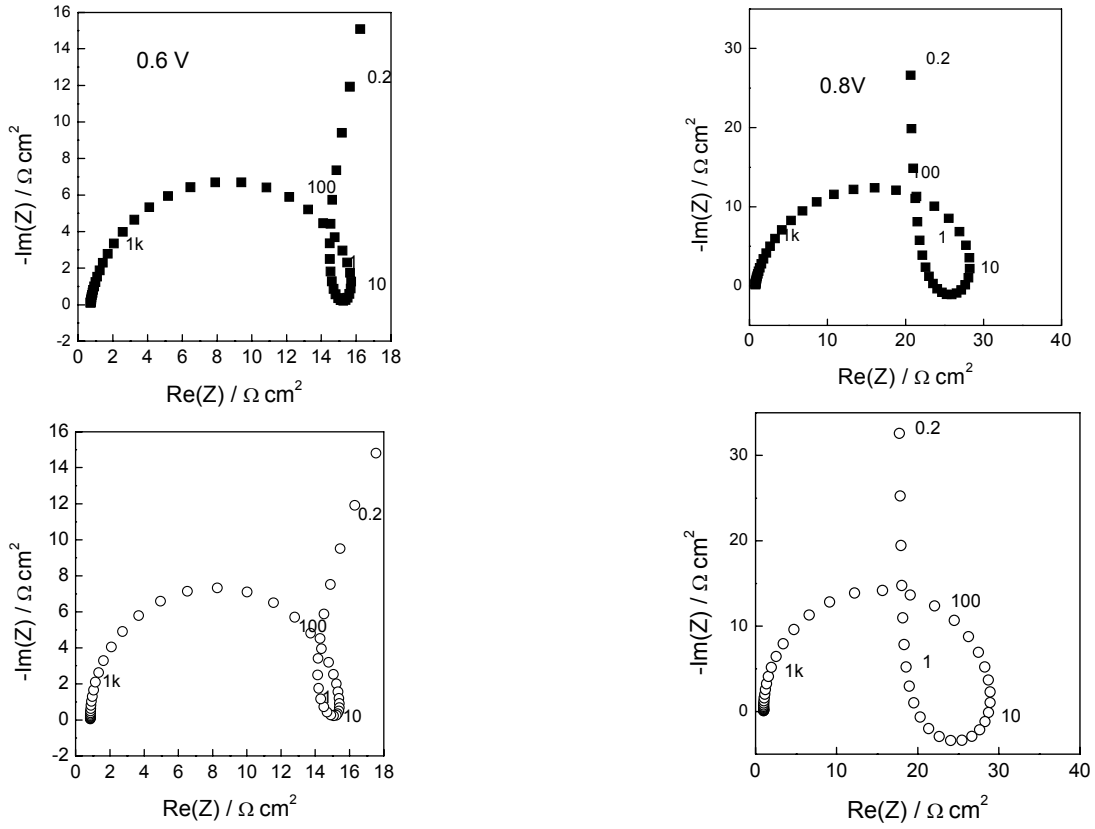

Fig. 3**.** Impedance spectra of W in 1 M SO_4^{2-} + 0.1 M F^-, pH 5 solution at 0.6 and 0.8 V. Closed symbols – experimental data, open symbols – best-fit calculation according to the proposed model. Parameter is frequency in Hz.

The oxide film resistance and capacitance dominate the impedance profile at high-frequencies. In the intermediate frequency range, a pseudo-inductive response becomes visible at potentials higher than 0.5 V, i.e. in general before the passivation peak, in analogy to earlier results with Nb in sulphate-fluoride electrolytes and Mo in phosphoric acid [46]. The appearance of such a response has been earlier ascribed to relaxation phenomena due to the formation and time variation of a negative surface charge at the oxide film/solution interface [44, 45]. This part of impedance spectra can be described by a low frequency time constant, $\tau_{LF} = R_{sc}.L_{sc}$. The value of this time constant (or the inverse of the characteristic frequency of the inductive loop) decreases with increasing pH, which indicates an accelerating effect on the build-up of the surface charge in the transient regime. The pseudo-inductive behaviour can be related to the increase of the rate of transport of dominating point defects (anion vacancies) across the oxide film, due to the presence of surface charge built up of the charge carriers of opposite sign. This approach was earlier confirmed by one of us for barrier film growth on tungsten in H_2SO_4 solution at potentials above the passivation peak [45]. At the low-frequency end, a further capacitive response was detected. In the active-to-passive transition region, it is most probably due to the passivation reaction since it tends to turn to a positive d.c. limit at potentials below ca. 0.5–0.7 V and to a negative d.c. limit at potentials above that value. In the passive region, the capacitive response at low frequencies can be due to the relaxation of film thickness with a.c. modulation, as it was proposed by a number of authors [45, 46, 59, 60]. Summarizing, the current versus potential curves and the a.c. impedance spectra in the passivation and passivity ranges of W in sulphate-fluoride solutions indicate a coupling between the dissolution of tungsten and the formation of a passivating oxide. In order to estimate in a quantitative way the kinetic and transport parameters pertinent to these two processes, an appropriate physico-chemical model has to be proposed. The next section is devoted to the detailed description of this model, which is based on an earlier approach to the passivation and passivity of Nb in sulphate-fluoride solutions [46].

DISCUSSION

Growth of the passive film and dissolution of tungsten

The oxide of tungsten that is formed at open circuit in an aqueous solution can be regarded as mixed-valency oxide [61], in which W(V) and W(VI) positions coexist in the cation sublattice, together with a certain concentration of W(VI) cation vacancies. A significant concentration of oxygen vacancies is assumed to exist in the anion sublattice as well. The W(V) cation vacancies are neglected for simplicity. The growth of the passive film [43, 49] proceeds at the metal/film interface with oxidation of the metal:

$$\mathrm{m} \rightarrow W_W + 3V_O^{\bullet\bullet} + 6e_m \qquad (1)$$

The oxygen vacancy is transported through the barrier film by high-field assisted migration and reacts with absorbed water at the film/solution interface achieving film growth:

$$3V_O^{\bullet\bullet} + 3H_2O \xrightarrow{k_4} 3O_O + 6H^+ \qquad (2)$$

In order to have film thickness invariant with time in the steady state, the film dissolution reaction must be included

$$WO_{3-x} + 2(3-x)H^+ \xrightarrow{k_d} W^{6+} + (3-x)H_2O \qquad (3)$$

In fluoride containing electrolytes, oxyfluoro-complexes of W(VI) are probably formed, which are expected to increase the solubility of the film and thus the steady-state current density is governed by chemical dissolution of the oxide. On the other hand, W(V) at the F/S interface undergoes either oxidative dissolution as W_{aq}^{6+} or is transformed into a passivating W(VI)* species that dissolves isovalently:

$$W_W^{V'} \xrightarrow{k_2} W_{aq}^{6+} + e' + V_W^{6'} \qquad (4)$$

$$\begin{aligned} W_W^{V'} &\xrightarrow{k_{31}} W_W^{VI*} + e' \\ W_W^{VI*} &\xrightarrow{k_{32}} W_{aq}^{6+} + V_W^{6'} \end{aligned} \qquad (5)$$

Cation vacancies, generated by the above processes, are transported through the film via hig-field assisted migration or recombine with oxygen vacancies according to the reaction:

$$V_O^{\bullet\bullet} + V_W^{6'} \rightarrow null \qquad (6)$$

The high-field migration equations for the transport of cation and anion vacancies are:

$$J_o = -\frac{D_0}{2a} c_O(L) e^{\frac{2FaE_0}{RT}}, \; J_M = c_M(0)\frac{D_M}{2a} \; e^{\frac{\chi FaE_0}{RT}} \qquad (7)$$

The total defect transport current density is $I = -2FJ_o + 6FJ_m$.

The electric field strength in the metal/oxide/electrolyte system $\vec{E}_0$ is given by the sum of all the potential drops in the system divided by the oxide film thickness [45]:

$$\vec{E}_0 = \left(\phi_{M/F} + \vec{E}L + \phi_{F/S}\right)/L \tag{8}$$

where $\phi_{M/F} = (1-\alpha)E - \vec{E}\,L$, $\phi_{F/S} = q_n L_{F/S}/\varepsilon\varepsilon_o$, α is the part of the applied potential, comsumed at the film/solution interface, as opposed to film bulk, q_n is the negative surface charge due to accumulation of cation vacancies at the film/solution interface, $\vec{E}$ is the field strength in the film bulk and $L_{F/S}$ is the width of the cation vacancy accumulation zone [45]. Further, according to the mixed-conduction model for oxide films [62], the potential drop at the metal/film interface does not depend on the applied potential. In other words, the reactions at this interface are not considered to be rate-limiting, rather, their rate is adjusted by transport processes of point defects in the passive film.

The expressions of the instantaneous partial currents due to the transport of oxygen and cation vacancies acquire the form:

$$I_0 = \frac{FD_0}{a}c_o(L)\ \exp\left\{\frac{2Fa}{RTL}\left[(1-\alpha)E + \frac{q_n L_{F/S}}{\varepsilon\varepsilon_0}\right]\right\},$$

$$I_M = \frac{6FD_0}{2a}c_M(0)\ \exp\left\{\frac{6Fa}{RTL}\left[(1-\alpha)E + \frac{q_n L_{F/S}}{\varepsilon\varepsilon_0}\right]\right\} \tag{9}$$

At the film/solution interface, the cation vacancies are (i) generated with a current density $I_{M,F/S}$, (ii) transported *via* high-field migration with a current density I_M and (iii) react with the oxygen vacancies according to the recombination reaction at a rate of $I_O S q_n$, where S is the cross-section of recombination. Then,

$$\frac{dq_n}{dt} = I_{M,F/S} - I_M - I_O S q_n = I_O S\left(\frac{I_{M,F/S} - I_M}{I_O S} - q_n\right) \tag{10}$$

According to the dissolution scheme, described by reactions (4) and (5), the current density due to cation vacancies at the film/solution interface is given by:

$$\frac{I_M}{6F} = J^{5'}{}_M = k_2\gamma_5 + k_{32}\gamma^*{}_6 \tag{11}$$

γ_5 and γ_6* being the fractions of the F/S interface, occupied by W(V) and W(VI)*, referred to the cation sublattice only. It is assumed that the surface concentration of W(V) cation vacancies can be disregarded with respect to γ_5 and γ_6*. The material balances in the outermost cation layer are correspondingly:

$$\frac{\beta d\gamma_5}{dt} = \frac{I_M}{6F} - k_2\gamma_5 - k_{31}\gamma_5 \tag{12}$$

$$\frac{\beta d\gamma_6{}^*}{dt} = k_{31}\gamma_5 - k_{32}\gamma_6{}^* \tag{13}$$

Steady state solution and total current density

In the steady state, Eqns. (12) and (13) become

$$\frac{\bar{I}_{M,F/S}}{6F} - \bar{k}_2\bar{\gamma}_5 - \bar{k}_{31}\bar{\gamma}_5 = 0 \tag{14}$$

$$k_{32}\bar{\gamma}_5 - \bar{k}_{31}\bar{\gamma}_6{}^* = 0 \tag{15}$$

and obviously

$$\bar{\gamma}_5 + \bar{\gamma}_6^* + \bar{\gamma}_6 = 1 \tag{16}$$

$\bar{\gamma}_6$ is the surface fraction occupied by WO_3, i.e. regular W(VI) sites, at which the isovalent dissolution of the oxide (reaction (3)) proceeds.

Eqns. (11), (15) and (16) can be used to calculate $\bar{I}_{M,F/S}$:

$$\bar{I}_{M,F/S} = \frac{6Fk_{32}\left(\bar{k}_2 + \bar{k}_{31}\right)}{\bar{k}_{31} + \bar{k}_{32}}\left(1-\bar{\gamma}_6\right) = \bar{k}_M\left(1-\bar{\gamma}_6\right) \tag{17}$$

$\bar{I}_M$ is supposed to be proportional to the surface $\left(1-\bar{\gamma}_6\right)$ not occupied by regular W(VI), whereas $\bar{I}_O$ is assumed to flow only on the fraction $\bar{\gamma}_6$.

$$\bar{I}_O = 2Fk_d c^n_{H^+}\bar{\gamma}_6 = 2Fk_d{}'\bar{\gamma}_6 = k_{WO_3}\bar{\gamma}_6 \tag{18}$$

where n is the reaction order of the chemical dissolution [Eqn. (3)] with respect to H^+.

If we define $\bar{\gamma}_6$ as a function of the reaction rates for the formation of W(V) and W(VI) sites

$$\bar{\gamma}_6 = \frac{k_{WO_3}}{\bar{k}_M + k_{WO_3}} \tag{19}$$

then

$$\bar{I}_M = \frac{\bar{k}^2{}_M}{\bar{k}_M + k_{WO_3}} \tag{20}$$

$$\bar{I}_O = \frac{\bar{k}^2_{WO_3}}{\bar{k}_M + k_{WO_3}} \tag{21}$$

Small amplitude a.c. solution

Based the assumption that currents, transported by oxygen and cation vacancies, are additive, and taking into account the electronic properties of the oxide, the impedance of the system can be defined as the parallel combination of the impedance due to generation and transport of cation vacancies (Z_M), the impedance due to transport and consumption of oxygen vacancies (Z_O) and the impedance due to the dielectric properties of the oxide film, i.e. its capacitance.

$$Z = R_{el} + \left[j\omega C + \frac{1}{Z_O} + \frac{1}{Z_M} \right]^{-1} \tag{22}$$

Here R_{el} is the electrolyte resistance and C is the film capacitance

$$C^{-1} = \frac{(1-\alpha)}{\varepsilon\varepsilon_0 \bar{E}} \bar{E} \tag{23}$$

Impedance due to transport and consumption of oxygen vacancies. For a small amplitude sinewave perturbation around a steady-state equation (10) transforms into:

$$\tilde{q}_n = \frac{\bar{I}_O S \alpha \tilde{E} \dfrac{\varepsilon\varepsilon_0}{L_{F/S}}}{j\omega + \bar{I}_O S}. \tag{24}$$

where $\tilde{x}$ indicates the complex amplitude of a variable x. The migration current of oxygen vacancies under such conditions is given by:

$$\tilde{I}_O = \frac{2\bar{I}_O B}{L}\left[(1-\alpha)\tilde{E} + \tilde{q}_n \frac{L_{F/S}}{\varepsilon\varepsilon_0} \right] \tag{25}$$

Solving (24) and (25) simultaneously, we obtain for the impedance of transport of oxygen vacancies the following:

$$Z_{O,f}^{-1} = \frac{\Delta I_0}{\Delta E} = \frac{2\bar{I}_0 B}{\bar{L}}\left[(1-\alpha) + \frac{\bar{I}_0 S\alpha}{j\omega + \bar{I}_0 S} \right] \tag{26}$$

In order to account for the capacitive behaviour, observed in the impedance spectra at low frequencies, the a.c. modulation of the film thickness has to be taken into account. The expression for the a.c. current density due to that phenomenon has the form:

$$\tilde{I} = \frac{(1-\alpha)}{\lambda \bar{E}} \frac{V_m}{6F} j\omega \tilde{E} \tag{27}$$

which corresponds to a pseudo-capacitance in series with the impedance due to transport of oxygen vacancies, $\lambda = \dfrac{\bar{I}_O}{\bar{I}_O + \bar{I}_M}$ is the current efficiency for film formation:

$$C_0 = \left(\bar{I}_O + \bar{I}_M\right)\frac{(1-\alpha)}{\bar{I}_O \bar{E}} \frac{V_m}{6F} \tag{28}$$

The total impedance due to oxygen vacancies is then expressed by:

$$Z_O = Z_{O,f} + \frac{1}{j\omega C_0} \tag{29}$$

Impedance due to generation and transport of cation vacancies. The Faradaic impedance due to the generation of cation vacancies at the F/S interface is derived from Eqs. (11), (12) and (13):

$$Z_{M,F/S}^{-1} = 6F\left[\tilde{k}_2 \bar{\gamma}_5 + \bar{k}_2 \tilde{\gamma}_5 + k_{32} \tilde{\gamma}_6^* \right] \tag{30}$$

$$j\omega\beta\tilde{\gamma}_5 = \frac{Z_{M,F/S}^{-1}}{6F} - \tilde{k}_2\tilde{\gamma}_5 - \tilde{k}_2\bar{\gamma}_5 - \tilde{k}_{31}\bar{\gamma}_5 - \bar{k}_{31}\tilde{\gamma}_5 \tag{31}$$

$$j\omega\beta\tilde{\gamma}_6^* = \tilde{k}_{31}\bar{\gamma}_5 - \bar{k}_{31}\tilde{\gamma}_5 - k_{32}\tilde{\gamma}_6^*$$

$$\tilde{\gamma}_6^* = \frac{\bar{k}_{31}\tilde{\gamma}_5 + \tilde{k}_{31}\bar{\gamma}_5}{\beta j\omega + k_{32}} \tag{32}$$

$$\tilde{\gamma}_5 = \frac{Z_{M,F/S}^{-1}}{6F\left(\beta j\omega + \bar{k}_2 + \bar{k}_{31}\right)} - \frac{\bar{\gamma}_5\left(\tilde{k}_2 + \tilde{k}_{31}\right)}{\left(\beta j\omega + \bar{k}_2 + \bar{k}_{31}\right)} \tag{33}$$

$$Z_{M,F/S} = 6Fb_2\bar{k}_2\bar{\gamma}_5\left[1 + \frac{b_{31}\bar{k}_{31}\left(\bar{k}_2 - \bar{k}_{31}\right)}{\left(1 + j\left(\dfrac{\omega\beta\bar{k}_2 b_2}{b_2 k_{32}\bar{k}_2 + b_{31}\bar{k}_{31}^2}\right)\right)\left(b_2\bar{k}_2 k_{32} + b_{31}\bar{k}_{31}^2 + \bar{k}_{31}\bar{k}_2\left(b_2 - b_{31}\right)\right)} \right] \tag{34}$$

The impedance of the transport of cation vacancies is written in complete analogy to Eqn. (26) as follows:

$$Z_{M,f}^{-1} = \frac{\Delta I_M}{\Delta E} = \frac{6\bar{I}_M B}{\bar{L}}\left[(1-\alpha) + \frac{I_0 S\alpha}{j\omega + I_0 S}\right] \quad (35)$$

The total impedance, due to generation and transport of cation vacancies, Z_M, is then given by:

$$Z_M = Z_{M,f} + Z_{M,F/S} \quad (36)$$

Then the total impedance is calculated using equations (22), (23), (29) and (36).

Comparison with the experimental results

In order to obtain quantitative estimates of the kinetic and transport parameters of the model, the following two-step calculation procedure was adopted. First, the total current density versus potential curves have been fitted to the sum of Eqns. (20), (21) with k_2^0, b_2, k_{31}^0, b_{31}, k_{32} and k_d' as adjustable parameters. Second, keeping these values constant, the impedance spectra at potentials from 0.1 to 4 V have been fitted to the sum of equations (22), (23), (29) and (36), using $\vec{E}, \alpha, a, S, \beta$ as adjustable parameters, and assuming a dielectric constant ε = 54 and a molar volume V_m = 31 mol·cm^{-3} for the oxide phase of the passive film. The current versus potential curves, calculated by this best-fit procedure, are shown in Fig. 1 with solid lines, whereas the calculated spectra for each solution at a range of potentials are represented with open symbols in Figs. 2 and 3. The estimated values of the rate constants k_2^0, k_{31}^0, k_{32} and k_d', which are dependent on the pH of the solution, are shown in Fig. 4, whereas the remaining parameters are collected in Table 1. A satisfactory agreement for both the magnitude and the frequency distribution of the impedance is obtained within the whole potential range, indicating the validity of the proposed approach.

Table 1. Kinetic and transport parameters dependence on pH.

Parameter	pH 0	pH 1	pH 3	pH 5
b_2, V^{-1}	12.5	12.0	12.2	12.5
b_{31}, V^{-1}	13.1	13.0	14.0	13.8
β, nmol·cm^{-2}	0.44	0.15	1.90	4.8
a, nm	0.39	0.40	0.31	0.45
$\vec{E}$, mV·cm^{-1}	3.7	4.1	4.0	5.0
α	0.39	0.40	0.40	0.40
S, mC^{-1}·cm^2	6.8	27.0	14.5	38

The main discrepancies lie in the fact that at certain potentials the exact diameters of the two high-frequency loops are not matched with sufficient accuracy. While a better match could be achieved by allowing some of the above parameters to vary with potential during the fit, this was not considered appropriate due to the already large number of parameters involved in the calculation. It is encouraging that the whole set of data within a large potential range and in four solutions are reproduced with a rather homogeneous set of parameters. The part of the potential, consumed at the film/solution interface α, the exponential coefficients b_2 and b_{31} are independent of potential within the calculational error, preserving values typical for film covered electrodes (the corresponding transfer coefficients α2 and α31 are ca. 0.3–0.35). The values of the field strength are also well within the limits of the very high-field approximation used in the present approach.

The increase of the field strength with pH (Table 1) can be related to the higher rate of film formation (i.e. ionic current density) due to the higher rate of film dissolution at the higher pH value. The main effect of pH factor is on two groups of parameters – on one hand, on the rate constants k_2^0, k_{31}^0, k_{32}, k_d' and on the maximum surface concentration of W(VI)* sites β (characterizing the processes of oxidation at the film/solution interface and generation of cation vacancies, as well as the chemical dissolution of the film) and on the other, on the capture cross-section of recombination of cation and anion vacancies at the film/solution interface, S.

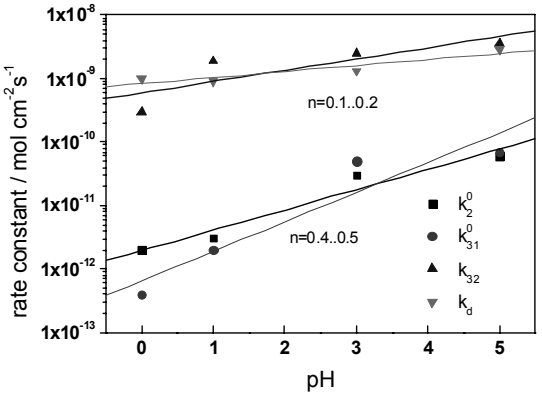

Fig. 4. Rate constants of the reactions of tungsten oxidation/dissolution at the oxide/electrolyte interface depending on the pH of the 1 M SO_4^{2-} + 0.1 M F^- solution.

The apparent reaction orders of the steps k_2^0, k_{31}^0, k_{32}, k_d' with respect to pH are given in the inserts of Fig. 4 and range between 0.4 and 0.5 (for k_2^0, k_{31}^0) and 0.1 and 0.2 (for k_{32}, k_d'). The orders with respect to pH are smaller than those with respect to fluoride in 1 M H_2SO_4, estimated earlier by us [63]. In other words, the effect of pH on the reaction

kinetics is of secondary importance in comparison to the effect of fluoride. The maximum surface concentration of W(VI)* sites β in general increases with pH indicating an increased defectiveness of the outermost layer of the oxide. The maximum surface concentration of cation vacancies can be related to the capture cross-section of recombination by the equation $S = (6F\beta_M)^{-1}$. The values of β_M, calculated from the S values represented in Table 1 are significantly smaller than the values of β. This validates aposteriori the decision to neglect the concentration of cation vacancies in the outermost layer compared to the regular W(V) and W(VI)* sites.

CONCLUSION

The following conclusions can be drawn based on the results, obtained in the present work:

The active-to-passive transition of W in 1 M SO_4^{2-} + 0.1 M F^- solution is the more prominent, the higher the pH of the electrolyte is. This fact can be tentatively related to the increased production of cation vacancies by an increasing non-stoichiometricity of the outermost layer of the oxide film. The reaction steps of W(V) oxidation into W(VI)* and its subsequent isovalent dissolution have reaction orders with respect to pH that are smaller than those with respect to fluoride, indicating that the pH has a secondary effect on the film dissolution, when compared to F^- addition.

In all studied electrolytes, the current density for W in the passive state is only slightly dependent on potential, indicating that the chemical dissolution of the oxide is probably the rate-controlling step of the overall oxidation process in this region. The steady-state current (i.e. the rate of the film dissolution reaction) increases with pH, which has been predicted also by the calculations on the basis of the proposed model.

The qualitative shape of impedance spectra is not affected by pH value. The impedance magnitude at low frequencies decreases with increasing pH value in accordance to the pH dependence of the steady state current density. The increase of the impedance magnitude at low frequencies with the potential can be explained by the effect of increasing film thickness with potential.

A quantitative kinetic model, involving film growth/dissolution processes at the film/solution interface and dissolution of tungsten through the oxide as parallel reaction paths, has been found to reproduce the steady-state current *versus* potential curves and the impedance spectra in a wide range of potentials and pH values. The pseudo-inductive feature at intermediate frequencies is explained by the interaction between two current carriers of opposite signs, which accelerates the transport of the major current carrier in the transient regime.

The main kinetic parameters of the model have been estimated and on the basis of their values hypotheses about the effect of pH on the respective rates of the processes of oxide film growth and tungsten dissolution through the forming oxide have been proposed. The main effect of pH factor is on the maximum concentration of cation sites and the cross-section of recombination of current carriers at the film/solution interface, which can be tentatively ascribed to the influence of pH on the defect structure of the outermost layer of the anodic film. Further investigations of the stoichiometry of the oxide layer are needed to confirm or reject this hypothesis.

***Acknowledgements**: The funding of this work by the National Science Fund, Bulgarian Ministry of Education and Science, under contract BY X-307/2007 is gratefully acknowledged.*

NOMENCLATURE

a	half-jump distance, cm;
b_i	coefficients of the interfacial reactions (i = 2,31), V^{-1};
C	capacitance of the barrier layer, $F \cdot cm^{-2}$;
C_O	pseudo-capacitance due to modulation of film thickness, $F \cdot cm^{-2}$;
D_O	diffusion coefficient of oxygen vacancies, $cm^2 \cdot s^{-1}$;
D_M	diffusion coefficient of cation vacancies, $cm^2 \cdot s^{-1}$;
E	applied potential, V;
$\vec{E}$	electric field strength, $V \cdot cm^{-1}$;
F	Faraday's constant, 96485 $C \cdot mol^{-1}$;
I	current density, $A \cdot cm^{-2}$;
I_M	current density due to cation vacancies, $A \cdot cm^{-2}$;
I_O	current density due to oxygen vacancies, $A \cdot cm^{-2}$;
J_M	flux of cation vacancies, $mol \cdot cm^{-2} \cdot s^{-1}$;
J_O	flux of oxygen vacancies, $mol \cdot cm^{-2} \cdot s^{-1}$;
j	imaginary unit;
k_i	rate constants of the interfacial reactions (i = 2, 31, 32, 4), $mol \cdot cm^{-2} \cdot s^{-1}$;
k_d	rate constant of the film dissolution reaction, $cm \cdot s^{-1}$;
k_M	constant defined in equation (18), $A \cdot cm^{-2}$;
k_{WO_3}	constant defined in equation (19), $A \cdot cm^{-2}$;
L	thickness of the barrier layer, cm;
$L_{F/S}$	thickness of the cation vacancy accumulation layer at the film/solution interface, cm;
m	tungsten atom in the metal phase;
$W^{V'}{}_W$	W(V) in a W(VI) position in the barrier film;
$W^{VI}{}_W$	W(VI) in a W(VI) position in the barrier film;

W^{VI*}_{W} W(VI) in a W (VI)* position in the outermost cation layer of the film;
O_O oxygen position in the barrier film;
$V_O^{\bullet\bullet}$ oxygen vacancy in the barrier film;
$V_W^{6'}$ tungsten cation vacancy in the barrier film;
S capture cross-section for a positive defect, $cm^2 \cdot C^{-1}$;
Z_M impedance due to cation vacancies, $\Omega \cdot cm^2$;
$Z_{M,f}$ impedance due to transport of cation vacancies in the film, $\Omega \cdot cm^2$;
$Z_{M,F/S}$ impedance due to cation vacancies at the film/solution interface, $\Omega \cdot cm^2$;
Z_O impedance due to oxygen vacancies, $\Omega \cdot cm^2$;
$Z_{O,f}$ impedance due to transport of oxygen vacancies in the film, $\Omega \cdot cm^2$;
q_n negative surface charge due to accumulation of cation vacancies, $C \cdot cm^{-2}$;
α polarizability of the film / solution interface;
α_i transfer coefficient ((i=2, 31) ;
β total number of cation positions per unit surface, $mol \cdot cm^{-2}$;
γ_5 fraction of W(V) in W(VI) positions in the outermost layer of the film;
γ_6 fraction of W(VI) in W(VI) positions in the outermost layer of the film;
γ_6* fraction of W(VI) in W(VI)* positions in the outermost layer of the film;
ε dielectric constant of the film;
ε_0 dielectric permittivity of vacuum, $F \cdot cm^{-1}$;
ω angular frequency, $rad \cdot s^{-1}$.

REFERENCES

1. A. Hamnett, in "Interfacial Electrochemistry - Theory, Experiment and Applications", Marcel Dekker, New York, 1999, Chap. 47, 871–873.
2. P. J. Barczuk, H. Tsuchiya, J. M. Macak, P. Schmuki, D. Szymanska, O. Makowski, K. Miecznikowski, P. J. Kulesza, *Electrochem. Solid State Lett.*, **9**, E13 (2006).
3. P. J. Kulesza, L. R. Faulkner, *J. Electroanal. Chem.*, **259**, 81 (1989).
4. P. K. Shen, A. C. C. Tseung, *J. Electrochem. Soc.*, **141**, 3082 (1994).
5. A. K. Shukla, M. K. Ravikumar, A. S. Arico, G. Candiano, V. Antonucci, N. Giordano, A. Hamnett, *J. Appl. Electrochem.*, **25**, 528 (1995).
6. M. Gotz, H. Wendt, *Electrochim. Acta*, **43**, 3637 (1998).
7. P. Kulesza, B. Grzybowska, M. A. Malik, M. Chojak, K. Miecznikowski, *J. Electroanal. Chem.*, **512**, 110 (2001).
8. L. X. Yang, C. Bock, B. MacDougall, J. Park, *J. Appl. Electrochem.*, **34**, 427 (2004).
9. J. Shim, C.-R. Lee, H.-K. Lee, J.-S. Lee, E. J. Cairns, *J. Power Sources*, **102**, 172 (2001).
10. H. Kawasaki, J. Namba, K. Iwatsuji, Y. Suda, K. Wada, K. Ebihara, T. Ohshima, *Appl. Surf. Sci.*, **41**, 547 (2002).
11. W. Gopel, K.D. Schierbaum, *Sens. Actuators B,* **26–27**, 1 (1995).
12. S. Badilescu, P. V. Ashrit, *Solid State Ionics*, **158**, 187 (2003).
13. E. Ozkan, S. H. Lee, P. Liu, C. E. Tracy, F. Z. Tepehan, J. R. Pitts, S. K. Deb, *Solid State Ionics*, **149**, 139 (2002).
14. A. E. Aliev, H. W. Shin, *Solid State Ionics* **154–155**, 425 (2002).
15. A. Antonaia, M. L. Addonizio, C. Minarini, T. Polichetti, M. Vittori-Antisari, *Electrochim. Acta*, **46**, 2221 (2001).
16. W. Cheng, E. Baudrin, B. Dunn, J. I. Zink, *J. Mater. Chem.,* **11**, 92 (2001).
17. C. G. Granqvist, *Electrochim. Acta*, **44**, 3005 (1999).
18. R. D. Rauh, *Electrochim. Acta*, **44**, 3165 (1999).
19. S. H. Lee, H. M. Cheong, J. G. Zhang, A. Mascarenhas, D. K. Benson, S. K. Deb, *Appl. Phys. Lett.* **74**, 242 (1999).
20. M. Sun, N. Xu, Y. W. Cao, J. N. Yao, E. G. Wang, *J. Mater. Res.* **15**, 927 (2000).
21. A. I. Gavrilyuk, *Electrochim. Acta*, **44**, 3027 (1999).
22. T. J. Coutts, X. Li, T. A. Cessert, *IEEE Electron. Lett.*, **26**, 660 (1990).
23. B. Stierna, C. G. Granqvist, *Appl. Opt.* **29**, 117 (1991).
24. A. DiPaola, F. DiQuarto, G. Serravalle, *J. Less-Common Met.,* **42**, 315 (1975).
25. I. P. Nenov, S. M. Ikonopisov, *Compt. Rend. Bulg. Acad. Sci.* **29**, 39 (1976).
26. A. DiPaola, F. DiQuarto, G. Serravalle, *Gazz. Chim. Ital.,* **106**, 277 (1976).
27. M. R. Arora, R. Kelly, *J. Electrochem. Soc.,* **124**, 1493 (1977)
28. M. R. Arora, R. Kelly, *J. Materials Sci.,* **12**, 1673 (1977).
29. A. DiPaola, F. DiQuarto, *Electrochim. Acta,* **22**, 63 (1977).
30. J. L. Ord, J. C. Clayton, K. Brudzewski, *J. Electrochem. Soc.*,**125**, 908(1978).
31. B. Reichman, A. J. Bard, *J. Electrochem. Soc.,***126**, 583 (1979).
32. A. DiPaola, F. DiQuarto, C. Sunseri, *Corr. Sci.,* **20**, 1067 (1980).
33. A. DiPaola, F. DiQuarto, C. Sunseri, *Corr. Sci.,* **20**, 1079 (1980).
34. F. DiQuarto, A. DiPaola, C. Sunseri, *J. Electrochem. Soc.,* **127**, 1016 (1980).
35. F. DiQuarto, A. DiPaola, C. Sunseri, *Electrochim. Acta,* **26**, 1177 (1981).
36. F. DiQuarto, G. Russo, C. Sunseri, A. DiPaola, *J. Chem. Soc. Faraday Trans. 1*, **78**, 3433 (1982).
37. M. M. Hefny, M. S. El-Basiouny, A. S. Mogoda, *Corrosion,* **39**, 266 (1983).
38. F. DiQuarto, S. Piazza, C. Sunseri, *J. Electroanal. Chem.,* **248**, 99 (1988).
39. F. DiQuarto, S. Piazza, C. Sunseri, *J. Electroanal.*

Chem., **248**, 117 (1988).
40. A. Goossens, D. D. Macdonald, *Electrochim. Acta,* **38**, 1965(1993).
41. A. Goossens, D. D. Macdonald, *J. Electroanal. Chem.,* **352**, 68 (1993).
42. S. R. Biaggio,R. C. Rocha Filho, J. R. Vilche, F. E. Varela, L. M. Gassa, *J. Braz.Chem. Soc.,*. **5**, 123 (1994)
43. E. Sikora, J. Sikora, D. D. Macdonald, *Electrochim. Acta,* **41**, 783 (1996).
44. S. R. Biaggio,R. C. Rocha Filho, J. R. Vilche, F. E. Varela, L.M. Gassa, *Electrochim. Acta,* **42**, 1751 (1997).
45. M. Bojinov, *Electrochim. Acta*, **42**, 3489 (1997).
46. M. Bojinov, S. Cattarin, M. Musiani, B. Tribollet, *Electrochim. Acta*, **48**, 4107 (2003)
47. K. Shimizu, G. M. Brown, H. Habazaki, K. Kobayashi, P. Skeldon, G. E. Thompson, G. C. Wood, *Corros. Sci.,* **40**, 1238 (1998).
48. D. D. Macdonald, E. Sikora, J. Sikora, *Electrochim. Acta*, **43**, 2851 (1998).
49. J. Sikora, E. Sikora, D. D. Macdonald, *Electrochim. Acta*, **45**, 1875 (2000).
50. M. Anik, K. Osseo-Asare, *J. Electrochem. Soc.*, **149**, B224 (2002).
51. M. Anik, *Turk. J. Chem.,* **26**, 915 (2002).
52. M. Metikos-Hukovic, Z. Grubac, *J. Electroanal. Chem.,* **556**, 167 (2003).
53. M.-G. Vergé, C.-O. A. Olsson, D. Landolt, *Corros. Sci.*, **46**, 2583 (2004).
54. C.-O. A. Olsson, M.-G. Vergé, D. Landolt, *J. Electrochem. Soc.*, **151**, B652 (2004).
55. M. Anik, *Corros. Sci.*, **48**, 4158 (2006).
56. O. K. Varghese, G. K. Mor, C. A. Grimes, *J. Mater. Res.,* **18**, 2296 (2003).
57. H. Tsuchiya, J. M. Macak, I. Sieber, L. Taveira, A. Ghicov, K. Sirotna, P. Schmuki, *Electrochem. Commun.*, **7**, 295 (2005).
58. R. Hahn, J.M. Macak, P. Schmuki, *Electrochem. Commun*. **9**, 947 (2007).
59. H. J. De Wit, C. Wijenberg, C. Crevecoeur, *J. Electrochem. Soc.,* **126**, 779 (1979).
60. L. Young, Ta-Ming Yang, C. Backhouse, *J. Electrochem. Soc.*, **142**, 3479 (1995).
61. Geonja Lim, Jong-Ho Lee, Ji-Won Son, Hae-Weon Lee, Joosun Kim, *J. Electrochem. Soc.*, **153**, B169 (2006).
62. M. Bojinov, G. Fabricius, T. Laitinen, K. Mäkelä, T. Saario, G. Sundholm, *Electrochim. Acta*, **45**, 2029 (2000).
63. V. Karastoyanov, M. Bojinov, *Mater. Chem. Phys.* (2007, in press)

ВЛИЯНИЕ НА pH НА ЕЛЕКТРОЛИТА ВЪРХУ МЕХАНИЗМА НА ПРОВОДИМОСТ НА АНОДНИТЕ ОКСИДНИ ФИЛМИ ВЪРХУ ВОЛФРАМ

В. И. Карастоянов, М. С. Божинов*

Катедра „Физикохимия“, Химикотехнологичен и металургичен университет, бул. „Кл. Охридски“ №8, 1756 София

Постъпила на 25 октомври 2007 г., Преработена на 9 февруари 2008 г.

(Резюме)

Анодното окисление на волфрама е изучено в 1 M сулфатни разтвори с pH от 0 до 5, съдържащи 0.1 M флуорид като HF или NaF. Стационарните плътности на тока в потенциалния интервал 0.1 до 4 V спрямо SCE нарастват с pH, което е указание за ускорено разтваряне на филма – необходимо условие за образуване на нанопорьозни оксидни структури. Така ефектът на добавките от флуорид върху стационарната плътност на тока е по-изразен в слабокисели разтвори, т.е. тези електролити са вероятно по-подходящи за получаване на системи от WO_3 нанотръбички. Електрохимичните импедансни спектри в областите на пасивация и пасивност са доминирани от процесите в бариерния слой и на неговата граница с електролита. Присъствието на псевдо-индуктивен полукръг в импедансните спектри при междинни честоти е указание за взаимодействие между точковите дефекти по време на процесите на растеж на филма и разтваряне на волфрам през него. Ниско-честотната капацитивна времекостанта вероятно е свързана със самия пасивационен процес. Предложеният кинетичен модел, включващ реакция на рекомбинация на положително и отрицателно натоварени точкови дефекти на границата филм/разтвор и кинетична схема на окислително разтваряне на волфрама на същата граница, описва адекватно стационарните токови плътности и импедансните спектри в зависимост от потенциала. Този модел на механизма на проводимост в бариерния подслой представлява съществена стъпка към количественото описание на формирането на нанопорьозен оксиден слой върху волфрам.